CHEMISTRY OF MATERIALS

Nanobodies and Antibodies for Duplexed EGFR/HER2 Immunoassays Using Terbium-to-Quantum Dot FRET

Xue Qiu,[†] K. David Wegner,[†,||] Yu-Tang Wu,[†] Paul M. P. van Bergen en Henegouwen,[‡] Travis L. Jennings,[§] and Niko Hildebrandt*,[†]

[†]NanoBioPhotonics (www.nanofret.com), Center for Nanoscience and Nanotechnology (C2N), Institute for Integrative Biology of the Cell (I2BC), Université Paris-Saclay, Université Paris-Sud, CNRS, CEA, 91405 Orsay Cedex, France

[‡]Cell Biology, Department of Biology, Science Faculty, Utrecht University, Utrecht, Netherlands

[§]Affymetrix, Inc., 10255 Science Center Drive, San Diego, California 92121, United States

S *Supporting Information*

ABSTRACT: Biosensors based on the combination of semiconductor quantum dots (QDs) and Förster resonance energy transfer (FRET) have demonstrated many advantages for simple, fast, sensitive, and multiplexed diagnostics. However, the implementation of QDs as functional standard materials into homogeneous (single-step) FRET immunoassays has not yet been accomplished, because profound investigations of antibody-conjugation strategies concerning their influence on diagnostic performance for quantifying clinical biomarkers are lacking. Here, we report about a systematic study of size, type, orientation, specificity, nonspecific binding, and cross-reactivity of antibodies conjugated to QDs for single and duplexed EGFR and HER2 immunoassays. Time-gated terbium-to-quantum dot FRET detection on a clinical immunoassay fluorescence plate reader (KRYPTOR) enabled a direct comparison of matuzumab, cetuximab, trastuzumab, and pertuzumab monoclonal antibodies and EgA1, EgB4, 11A4, and 18A12 V_HH nanobodies conjugated to 605 and 650 nm emitting QDs. Detection limits of 2.9 ng/mL EGFR, using cetuximab and matuzumab conjugates, and 8.0 ng/mL HER2, using oriented 11A4 and 18A12 conjugates, demonstrated the capability of detecting concentrations well below the clinical cutoff values. Multiplexed assays could quantify EGFR and HER2 at low nanomolar concentrations from the same sample. Our results show that careful optimization of QD-antibody conjugation is a prerequisite to implementing QDs into applied clinical diagnostics.
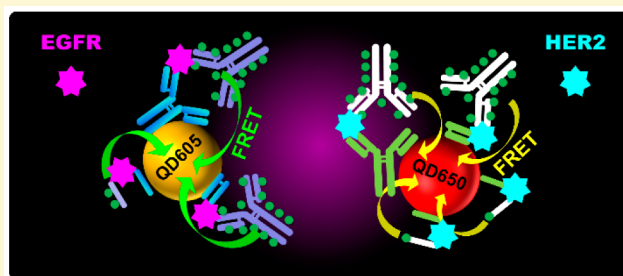
INTRODUCTION

The rapid development of clinical diagnostics in specialized areas, such as point-of-care testing and personalized medicine,[1−3] has led to an increasing demand for the simultaneous detection of different biomarkers from a single sample, so-called multiplexing.[4−6] In addition to multiplexing, the simplicity and rapidness of diagnostic tests are of paramount importance both temporally (time between sampling and clinical decision) and economically (costs of material and personnel). Homogeneous immunoassays, which do not require several incubation, washing, and separation steps but only simple mixing and incubation followed by the measurement,[7] are therefore much sought-after. One of the few optical techniques for homogeneous assays is based on Förster resonance energy transfer (FRET) from lanthanide−antibody to dye−antibody conjugates through specific recognition of a biomarker by both antibodies (ABs). Such assays have become standard techniques for diagnostics of various biomarkers[8−11] and are commercially available under brand names such as HTRF (Cisbio), TRACE (BRAHMS/ThermoFisher), or LANCE (PerkinElmer) for different fluorescence plate reader systems.

The design of homogeneous FRET immunoassays with multiplexing capability, and without compromising the high performance and reproducibility necessary for clinical diagnostics, is extremely challenging, because (*i*) several ABs (two per antigen) must provide high specificity for their respective biomarkers (with minimum nonspecific binding and cross-reactivity) and (*ii*) spectral crosstalk of the different fluorescent labels used for signal transduction must be avoided. Nanoparticles, such as quantum dots (QDs), allow for a versatile conjugation of various ABs of the same or different kind by several conjugation strategies,[12] and the outstanding photophysical properties of QDs can be very beneficial for both high sensitivity and multiplexed FRET diagnostics.[11,13] The tunable PL colors of QDs have been exploited within various multiplexed immunoassay applications, such as multicolor microbead detection[14] or multicolor QD detection on functional microporous membranes.[15] Also, different lanthanide
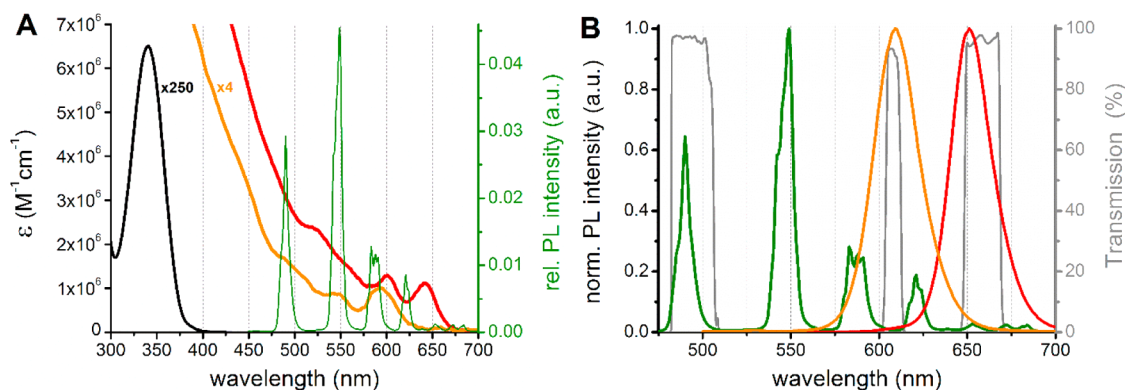
Figure 1. Absorption (extinction coefficients ε, A) and emission (normalized photoluminescence (PL) intensity, B) spectra of Tb (black for absorption, green for PL) and QDs (orange for QD605 and red for QD650). For better visibility, the absorption spectra of Tb and QD605 were multiplied by 250 and 4, respectively. The PL spectrum of Tb in A served for the calculation of the FRET overlap integral. The gray spectra in B show the transmission of the optical bandpass filters within the Tb (494 ± 12 nm), QD605 (608 ± 4 nm), and QD650 (659 ± 10 nm) detection channels.[21]

ions, such as Eu^{3+} in combination with Sm^{3+}, were used for multiplexed immunoassays.[16] However, all of these technologies are heterogeneous, which means that several, often time-consuming, immobilization, washing, incubation, and separation steps are necessary for the complete assay procedure. Simple and rapid single-step (homogeneous) immunoassays that used FRET from terbium complexes (Tb) to QDs were applied against different targets, such as alpha-fetoprotein (AFP),[17] carcinoembryonic antigen (CEA),[18,19] prostate-specific antigen (PSA),[20,21] and the epidermal growth factor receptor EGFR.[22] In an earlier study, we demonstrated multiplexed Tb-to-QD FRET using the prototypical biotin–streptavidin binding system for five different Tb/QD FRET pairs.[23] Beyond these important proofs-of-concept, two highly important milestones for a successful implementation of QDs into homogeneous and multiplexed immunoassays for clinical use would be (*i*) to understand the diagnostic performance of QD conjugation with ABs of different types, sizes, and orientations on the QD surfaces and (*ii*) the actual accomplishment of a homogeneous multiplexed assay, i.e., the one-step detection of different biomarkers from a single sample.

In the present study, we investigated duplexed Tb-to-QD FRET immunoassays using the epidermal growth factor receptors EGFR and HER2 as model biomarkers. Both are cell surface receptor tyrosine kinases that transduce cell proliferation and survival signals through dimerization with HER family receptors, and an aberrant regulation of these receptors has been implicated in a broad range of human malignancies such as lung and breast cancers.[24−26] Taking into account the diverse expression levels of HER2 and EGFR for these types of cancer and the fact that heterodimerization of HER2 and EGFR has quantitative and qualitative implications on the signaling output,[27−30] duplexed detection of these receptors could be an important diagnostic tool for personalized cancer therapy.[31] Commercially available enzyme linked immunosorbent assays (ELISA) against human soluble EGFR (e.g., by abcam) and HER2 (e.g., by Aviscera Bioscience) already provide detection limits in the low picogram per milliliter concentration range, which is far below the clinical cutoff levels (concentration threshold for the distinction between normal and abnormal concentrations) of 45 ng/mL and 15 ng/mL for EGFR and HER2, respectively.[27,30] However, these assays are heterogeneous

(require several time-consuming incubation and washing steps) and a duplexed assay for both EGFR and HER2 does not exist. Moreover, much higher EGFR and HER2 concentrations (in the tens to hundreds of ng/mL) have been found for cancer patients and healthy controls within clinical studies.[27,30] A simple and quick homogeneous assay with higher detection limits but with the capability of duplexed detection may therefore be an excellent diagnostic tool for initial screening that can provide a fast decision concerning the application of more complicated tests and histological analysis. Because EGFR and HER2 are structurally related, their duplexed detection sets high demands for the specificity of the ABs. Application of different bioconjugation strategies and a systematic investigation of diagnostic performance, using therapeutic monoclonal full size ABs (IgG), fragmented ABs (Fab), and single domain ABs (nanobodies or V_HH fragments), allowed for a direct comparison of the various AB–QD conjugates and showed that size, orientation, nonspecific binding, and cross-reactivity of the different ABs are important parameters that need to be taken into account for finding the optimal nanobiomaterial combination. Moreover, we demonstrated the first homogeneous, duplexed Tb-to-QD FRET immunoassay, which was able to detect two different targets (both EGFR and HER2) from a single 50 μL sample at low nanomolar concentrations.

RESULTS AND DISCUSSION

Antibody Conjugates. An ideal AB–QD conjugation for FRET immunoassays would include control over size, ratio of AB per QD, and orientation of the ABs on the QD surface. Moreover, the optimal photophysical properties of the QD and biological activity of the AB should not be compromised within the AB–QD conjugate.[32] These properties, in turn, determine the brightness, sensitivity, and specificity of the AB–QD conjugate and the distance to the FRET donor (or acceptor) ABs, i.e., the FRET efficiency. Commonly used bioconjugation strategies often lead to AB unfolding and random orientation on the surface of QDs,[33] which decreases the performance of the AB–QD conjugates. Evaluating the influence of size, ratio, and orientation of ABs, size and color of QDs, and type of biomarker, under comparable conditions, requires the conjugation of various ABs to different QDs using the same conjugation strategy and the application of these AB–QD

Scheme 1. Combination of Different Types of Antibodies against EGFR and HER2 and Different Orientations of V_HH (Oriented Conjugation via a Terminal Cysteine or Random Orientation via Amine-Conjugation) Allowed for Many Combinations of FRET Sandwich Immunoassays[a]
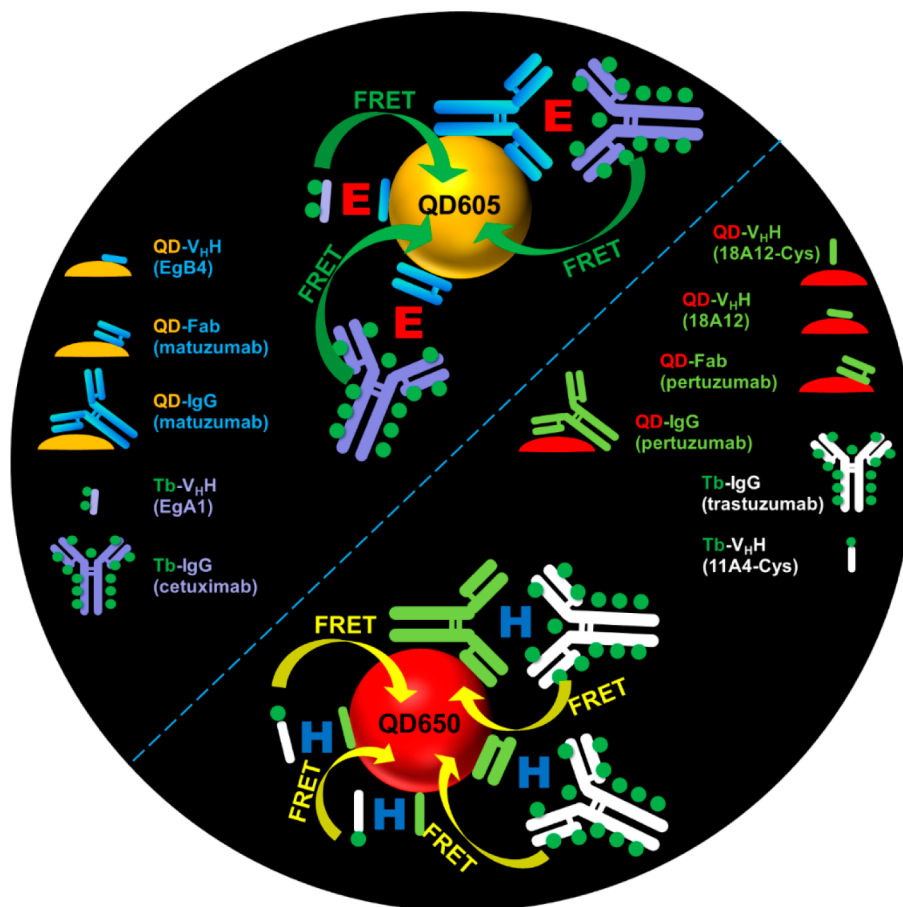
[a]Green dots symbolize Tb. The examples show QD605 for EGFR (E) and QD650 for HER2 (H) detection. However, both QDs were used for both biomarkers. The depicted differences in sizes of the various materials are not to scale.

conjugates to the detection of different biomarkers. This approach also necessitates the conjugation of the corresponding FRET donor (or acceptor) ABs. To realize such an extensive characterization, we selected the following biological and photonic materials for our Tb-to-QD FRET immunoassays:

1. Biomarkers (Targets). EGFR and HER2 (both ErbB receptors).

2. Antibodies. Immunoglobulin G (IgG) ABs: Matuzumab (Mat) and cetuximab (Cet), which are both Merck therapeutic humanized monoclonal IgGs against different epitopes of EGFR; pertuzumab (Pert) and trastuzumab (Tras), which are both Genentech/Roche therapeutic humanized monoclonal IgG ABs against different epitopes of HER2.

Fragment antigen-binding (Fab) ABs: Matuzumab (MatFab) and pertuzumab (PertFab).

V_HH nanobodies: EgA1 and EgB4, which are both V_HH against different epitopes of EGFR,[34] and 18A12 and 11A4 (both with a C-terminal cysteine group), which are both V_HH against different epitopes of HER2.[35]

3. Terbium FRET Donors (Figure 1). Tb (NHS- or maleimide-functionalized Lumi4-Tb complex).

4. QD FRET Acceptors (Figure 1). QD605 (maleimide-functionalized eBioscience/Affymetrix QD with an emission maximum at 605 nm and a diameter of 6.1 nm for the CdSe/ZnS nanocrystal) and QD650 nm (maleimide-functionalized

eBioscience/Affymetrix QD with an emission maximum at 650 nm and a diameter of 8.7 nm for the CdSe/ZnS nanocrystal).[36]

IgG, Fab, and V_HH conjugates were prepared using sulfhydryl-reactive chemistry for AB−QD conjugates (for V_HH, amino groups were transferred into sulfhydryl groups via a cross-linker) and amino-reactive or sulfhydryl-reactive chemistry for the Tb−AB conjugates, because these conjugation strategies were shown to be functional in different Tb-to-QD FRET immunoassays.[21,22] Compared to IgGs, nanobodies were shown to offer a better control of orientation, as they can be manipulated with terminal modifications, such as cysteines, using standard molecular biology techniques.[33] Therefore, 18A12 and 11A4 V_HH with C-terminal cysteine groups were directly conjugated with maleimide-functionalized QDs and Tb, respectively. The different AB types, sizes (∼150 kDa for IgGs, ∼50 kDa for Fab, and ∼15 kDa for V_HH), and orientations (C-terminal and random) provided a large variability for our comparative study, as schematically outlined in Scheme 1. It should be noted that we did not use Tb−Fab conjugates, because Fab is not expected to display any advantages compared to IgG for Tb conjugation (fewer Tb donors can be conjugated to a Fab). On the other hand, Fab−QD conjugation has two important advantages over IgG−QD conjugation. First, the smaller Fab allows for a higher conjugation ratio to QDs. Second, the separation of free Fab

Table 1. Tb−AB and AB−QD Conjugates and Conjugation Ratios (as Determined by Linear-Combination of Tb, QD, and AB Absorption Spectra)[a]

EGFR conjugates			HER2 conjugates		
AB type	**Tb conjugates**	**Tb/AB**	**AB type**	**Tb conjugates**	**Tb/AB**
V_HH	Tb-EgA1	2	V_HH	Tb-Cys11A4	1
IgG	Tb-Mat	4	IgG	Tb-Tras	14
IgG	Tb-Cet	8	**AB type**	**QD conjugates**	**AB/QD**
AB type	**QD conjugates**	**AB/QD**	V_HH	18A12Cys-QD650	20
V_HH	EgB4-QD605	22	V_HH	18A12-QD650	17
V_HH	EgB4-QD650	18	V_HH	18A12Cys-QD605	10
Fab	MatFab-QD605	14	V_HH	18A12-QD605	3*
Fab	MatFab-QD650	36*	Fab	PertFab-QD605	3*
IgG	Cet-QD650	4	Fab	PertFab-QD650	17
IgG	Mat-QD605	4	IgG	Pert-QD605	3
IgG	Mat-QD650	7	IgG	Pert-QD650	8

average V_HH per QD	17±9
average Fab per QD	16±8
average IgG per QD	5±3

[a]An asterisk (*) denotes outliers with conjugation ratios beyond the deviation from the average. Such strong deviations are caused by the extremely high absorbance values of QDs at 280 nm (~6.3×10^6 M^{-1} cm^{-1} for QD605 and ~3.2×10^7 M^{-1} cm^{-1} for QD650) compared to the ones of V_HH (~3.2 to 3.7×10^4 M^{-1} cm^{-1}), Fab (7.0×10^4 M^{-1} cm^{-1}), and IgG (2.1×10^5 M^{-1} cm^{-1}). Therefore, some samples, and, in particular, those of V_HH and Fab QD conjugates, for which the difference is highest, led to relatively low precision measurements.
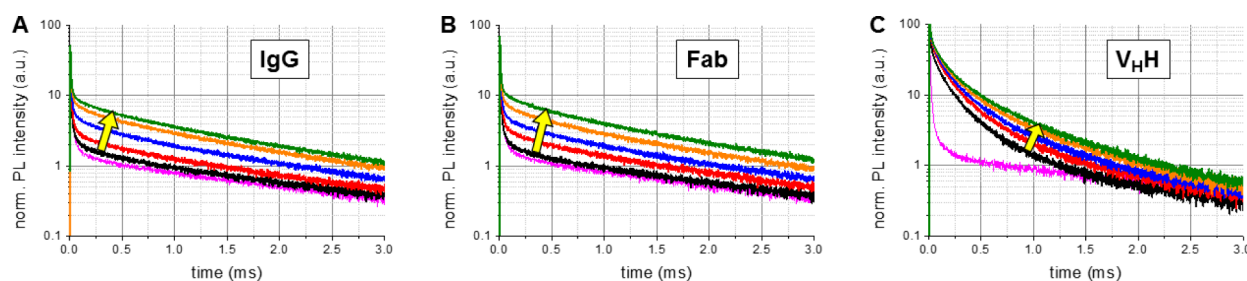

Figure 2. Representative normalized PL intensity decay curves (measured at 659 ± 10 nm) of AB−QD and Tb−AB conjugates mixed with increasing concentrations of EGFR (0 nM, black; 0.9 nM, red; 2.25 nM, blue; 4.5 nM, orange; and 9 nM, green) for the Tb-Cet/Mat-QD650 (A), Tb-Cet/MatFab-QD650 (B), and Tb-EgA1/EgB4-QD650 (C) FRET pairs. Yellow arrows indicate QD FRET sensitization with increasing EGFR concentration. The magenta curves present the mathematical sum of only AB-QD650 and only the Tb−AB conjugate. Although the optical bandpass filters (cf. Figure 1B) were selected to minimize Tb crosstalk into the QD detection channels, there was still significant Tb PL detectable. For intensity normalization, all curves within one graph where multiplied by the value that led to unity intensity for the magenta curve at 0.5 ms. PL decay curves (Tb donors and QD acceptors) of all immunoassays can be found in the Supporting Information (Supporting Figures S1−S8).

from Fab−QD conjugates is much easier, because Fab is approximately 3 times smaller than IgG. An overview of all Tb and QD conjugation methods, including conjugation reagents, reaction groups, and specific treatments for each conjugate, is summarized in Supporting Table S1.

Because the sizes of the Fab (ca. 50 kDa and 4 nm × 5 nm × 8 nm)[37] and V_HH (ca. 15 kDa and 2.5 nm × 2.5 nm × 4 nm)[38] are significantly smaller than that of IgG (ca. 150 kDa and 6 nm × 9.5 nm × 15 nm),[39] it was expected that the conjugation ratios were significantly lower for Tb per Fab or per V_HH or higher for Fab or V_HH per QD. This expectation could be confirmed by absorption measurements of 20 different EGFR and HER2 AB conjugates (Table 1). Although the differences in the absorption spectra of QDs and AB−QD conjugates are not easily distinguishable (due to the extremely large extinction coefficients of QDs in the UV, cf. footnote in Table 1), which can lead to significant errors, the measurement of many different conjugates clearly showed higher conjugation ratios for Fab and V_HH compared to IgG QD conjugates (Table 1). Also, the Tb conjugation ratios were much lower for V_HH

compared to Tb−IgG conjugates (Tb−Fab conjugates were not used).

Time-Resolved PL Analysis. Homogeneous FRET immunoassays against EGFR with seven different combinations of ABs and QDs (two colors) were investigated on a time-resolved fluorescence plate reader (Edinburgh Instruments). All 150 μL samples contained 50 μL of each AB conjugate (Tb and QD) at constant concentrations and 50 μL of EGFR at increasing concentrations. The PL decay curves, and, in particular, those of the QD acceptors, provided much useful information about the QD sensitization via FRET from Tb during the immunoassays. Because the Tb−AB and AB−QD concentrations were the same in all samples, an increasing EGFR concentration led to increasing sensitization (more donor−acceptor pairs) at constant FRET efficiency (donor−acceptor distance did not change). Figure 2 shows normalized QD650 PL decay curves for the IgG system (Tb-Cet and Mat-QD650), the Fab system (Tb-Cet and MatFab-QD), and the V_HH system (Tb-EgA1 and EgB4-QD), for which the increasing sensitization becomes clearly visible in the PL intensities of the decay curves. Similar results were found for

the different HER2 immunoassays configurations (Supporting Figure S9).

The time-resolved immunoassay analysis also provided valuable insights into nonspecific binding of the different ABs. For EGFR, the V_HH system without any EGFR (black curve in Figure 2C) already showed significant FRET sensitization from Tb. This presensitization was related to nonspecific binding of the nanobodies to bovine serum albumin (BSA), which is an essential component in all immunoassays. Therefore, the Tb-EgA1 and EgB4-QD were already brought in close proximity via BSA, which led to FRET even in the absence of EGFR. As the specific recognition of EGFR for both of these V_HH conjugates was stronger than nonspecific BSA binding, the addition of EGFR still led to the typical EGFR concentration-dependent sensitization. Previous studies showed the same phenomenon,[22] and therefore this presensitization was not unexpected. Interestingly, the anti-HER2 V_HH immunoassay systems did not show any presensitization (Supporting Figure S9), suggesting the complete absence of nonspecific binding to BSA. In contrast to the anti-EGFR V_HH, which contained histidine-tags for purification, both 11A4 and 18A12 were tagless V_HH. We therefore believe that the histidine tag is responsible for the nonspecific binding to BSA, although further studies are necessary to confirm this assumption. The IgG and Fab systems showed significantly less nonspecific binding (black compared to magenta curves in Figure 2A and B and Supporting Figure S9), which was stronger for IgG than for Fab and more significant for the anti-HER2 compared to the anti-EGFR ABs.

Depending on the type of AB used for the assays, the donor−acceptor distance was also expected to be different. Despite the large difference in sizes between IgG and Fab, the PL decay curves did not reveal any significant difference in PL decays (Figure 2A and B), whereas the V_HH system (Figure 2C) revealed much shorter decay times. These findings were again confirmed by the time-resolved HER2 immunoassays (Supporting Figure S10). For each EGFR system, we analyzed six different (between 4.5 and 12 nM EGFR) FRET-sensitized QD650 decay curves using a previously developed fitting procedure for Tb-sensitized acceptor decays.[40] Decay times of the donor in the absence of the acceptor (τ_D) and Förster distances (R_0) varied slightly between the three immunoassay systems because of the different influences of the ABs on the Tb decays. For the small V_HH, Tb was not significantly quenched, which led to a monoexponential decay with $\tau_D(V_HH) = 2.70 \pm 0.05$ ms and $R_0(V_HH) = 11.1 \pm 0.5$ nm. Conjugation of Tb to IgG quenched the overall Tb PL (8 Tb/AB) by ca. 20%, which led to multiexponential decays with an amplitude averaged decay time of $\langle\tau_D(IgG)\rangle = 2.15 \pm 0.10$ ms and $R_0(IgG) = 10.7 \pm 0.8$ nm. Using the FRET efficiency equation (eq 1) and the amplitude averaged decay times of the donor in the presence of the acceptor (FRET decay times) of $\langle\tau_{DA}(IgG)\rangle = 1.2 \pm 0.1$ ms, $\langle\tau_{DA}(Fab)\rangle = 1.2 \pm 0.1$ ms, and $\langle\tau_{DA}(V_HH)\rangle = 0.48 \pm 0.05$ ms, the average donor−acceptor (Tb−QD650) distances were $r(IgG) = 11.0 \pm 1.5$ nm, $r(Fab) = 11.0 \pm 1.5$ nm, and $r(V_HH) = 8.6 \pm 0.8$ nm. It should be noted that our FRET systems were comprised of multiple Tb donors per QD acceptor. Such multiple-donor/one-acceptor systems do not alter the FRET-efficiency (E_{FRET}) compared to a one-donor/one-acceptor system. However, due to the much longer excited-state lifetimes of Tb compared to QD, they increase the probability of QD-acceptor sensitization.[11]

$$E_{FRET} = \frac{R_0^{\,6}}{R_0^{\,6} + r^6} = 1 - \frac{\tau_{DA}}{\tau_D} \tag{1}$$

The distance values determined by FRET were in good agreement with the QD shape and size (ca. 9 nm radius if approximated as a sphere),[36,41] the random labeling of Tb on the ABs and the variable orientation of the (AB-QD)-EGFR-(Tb−AB) sandwich complexes, and the much shorter V_HH (compared to IgG and Fab) that can lead to very close Tb to QD-surface distances. Although one may expect larger distances for IgG compared to Fab, the facts that (i) both were conjugated via sulfhydryl groups (reduced cysteines) to the QDs, which led to much less random orientation compared to labeling via amino groups and therefore a similar orientation of IgG and Fab on the QD, (ii) the flexibility of ABs,[42] and (iii) the use of Tb-IgG ABs with 8 Tb/Cet (cf. Table 1) as donors in both cases, explain the similar average donor−acceptor distances for IgG and Fab. These results show that from the distance-point-of-view there is no reason to prefer Fab versus IgG (at least for the conjugation strategy used here). For the V_HH system, the donor−acceptor distance was significantly (ca. 2.4 nm) shorter because both Tb−V_HH and V_HH−QD were used in this system. Therefore, the V_HH-based FRET immunoassay (Tb-EgA1-EGFR-EgB4-QD650) provided better FRET efficiencies (ca. 80%) compared to the Fab (Tb-Cet-EGFR-MatFab-QD650) and IgG (Tb-Cet-EGFR-Mat-QD650) assays (ca. 60%).

EGFR Immunoassays. To evaluate and compare the diagnostic performance of all EGFR immunoassay configurations, immunoassay calibration curves (Figure 3) were acquired on a KRYPTOR compact plus (Cezanne/BRAHMS/
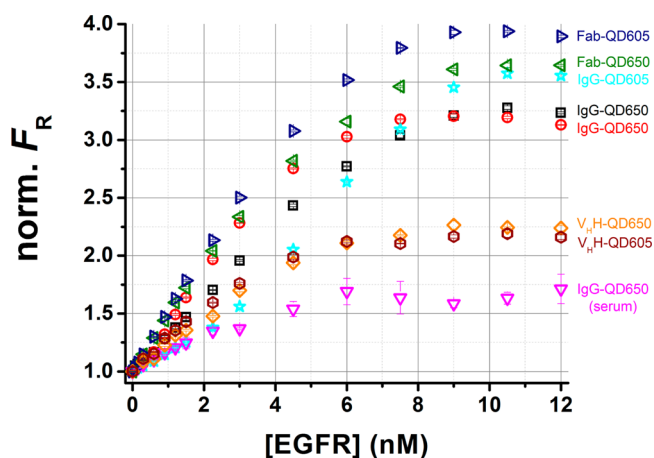
Figure 3. Homogeneous FRET immunoassay calibration curves against EGFR using different Tb−AB and AB−QD conjugates (blue, Tb-Cet/MatFab-QD605; green, Tb-Cet/MatFab-QD650; cyan, Tb-Cet/Mat-QD605; black, Tb-Mat/Cet-QD650; red, Tb-Cet/Mat-QD650; orange, Tb-EgA1/EgB4-QD650; brown, Tb-EgA1/EgB4-QD605; magenta, Tb-Cet/MatFab-QD650 measured in serum samples). [EGFR] corresponds to the variable EGFR dimer concentrations (recombinant human EGFR Fc chimera) in the 50 μL EGFR samples (in buffer or serum), whereas the overall measuring volume of 150 μL also contained 100 μL of a constant assay solution (50 μL of Tb−AB conjugate with 9 nM AB and 50 μL of AB−QD conjugate with 1.5 nM of QD650 or 3 nM of QD605 for all samples). Individual curves for the Tb and QD signals (that lead to the calculation of F_R) and for the determination of LODs can be found in the Supporting Information (Supporting Figures S11−S18).

Thermo Fisher Scientific) clinical fluorescence plate reader, which simultaneously detected the time-gated PL intensities (integration of the PL intensities within the time window from 0.1 to 0.9 ms after pulsed excitation) of the Tb donor (I_{Tb}) and the QD acceptor (I_{QD}). The FRET ratio $F_R = I_{QD}/I_{Tb}$ (and F_R normalized to unity for zero biomarker concentration) was used for the determination of the EGFR concentration. All assay curves showed a strong increase of F_R (caused by QD FRET-sensitization from the Tb donors) with increasing EGFR concentrations from 0.075 nM to *ca.* 9 nM EGFR. At higher EGFR concentrations, all Tb−ABs were saturated by EGFR and the calibration curves leveled off. The inflection points of the calibration curves were around 4 to 5 nM EGFR, which was in excellent agreement with the concentration of the Tb−ABs (EGFR monomer concentration is 8 to 10 nM in that case). At EGFR concentrations beyond 12 nM (not shown), F_R decreased due to the "hook effect" (more single EGFR−AB complexes than AB−EGFR−AB sandwich complexes).[18] The relatively small dynamic range of approximately 2 orders of magnitude (0.075−9 nM) can be significantly increased by kinetic measurements (from the very beginning of incubation of EGFR and AB-conjugates) and automatic dilution. The KRYPTOR clinical plate reader provides such an automatic dilution mode,[21] a very useful option in breast cancer diagnostics, for which soluble EGFR concentrations in the 10 to 120 ng/mL were found.[27,30]

The sensitivity of an immunoassay is determined by the slope of its calibration curve. The general trend of the curves from Figure 3 showed the highest sensitivity for Fab, followed by IgG and then V$_H$H. Although the average donor−acceptor distances for the IgG and Fab systems were similar (*vide supra*), the higher sensitivity of Fab can be explained by the higher conjugation ratio of Fab/QD compared to IgG/QD, which led to more Tb donors per QD acceptor in the case of Tb-IgG-EGFR-Fab-QD sandwich formation and confirmed previous results for PSA FRET immunoassays.[21] Despite the high conjugation ratios of V$_H$H/QD, the lower sensitivities of the V$_H$H-based assays were mainly related to the nonspecific binding (*vide supra*). Another aspect may be that Cet and Mat bind to the same domain of EGFR (domain III),[43] whereas EgA1 and EgB4 bind to different domains (domain III and domain I, respectively).[34,44] To include a direct buffer/serum comparison in our study, we used the Tb-Cet-EGFR-Mat-QD650 assay as a representative system. The sensitivity (slope) in buffer (red data points) was approximately 2-fold higher compared to serum (magenta data points).

Perhaps even more important than sensitivity is the limit of detection (LOD), which should be ideally below the clinical cutoff level (distinction between normal and abnormal biomarker concentrations) of the biomarkers. LODs are usually determined as the concentration corresponding (on the calibration curve) to the signal intensity of the assay without any biomarker (zero concentration) plus 3 times its standard deviation. In our case, we used 30 different measurements of the zero concentration sample for determining the standard deviation. Table 2 shows an overview of LODs, which were all significantly below the recommended cutoff level of 45 ng/mL EGFR.[27,30] Moreover, the lowest LODs for the Fab systems, followed by IgG and then V$_H$H confirmed the general trend found for sensitivity.

HER2 Immunoassays. Similar to the EGFR assays, we studied the various Tb−AB and AB−QD conjugates (Table 1) for their performance in homogeneous HER2 immunoassays.

Table 2. Limits of Detection (LODs) of the Different EGFR Immunoassays

AB combination	AB conjugate combination	LOD (nM)	LOD (ng/mL)	LOD (fmol)
IgG/IgG	Tb-Mat/Cet-QD650	0.04	8.3	2.1
	Tb-Cet/Mat-QD650	0.02	4.4	1.1
	Tb-Cet/Mat-QD650 (serum)	0.04	7.1	1.8
	Tb-Cet/Mat-QD605	0.07	13.9	3.5
IgG/Fab	Tb-Cet/MatFab-QD650	0.01	2.9	0.7
	Tb-Cet/MatFab-QD605	0.02	4.8	1.2
V$_H$H/V$_H$H	Tb-EgA1/EgB4-QD650	0.12	23.9	6.0
	Tb-EgA1/EgB4-QD605	0.11	22.9	5.7

An important additional feature of the HER2 assays was the investigation of oriented versus nonoriented V$_H$H−QD conjugation. Tb was conjugated to the C-terminal cysteine of 11A4 within all assays, whereas 18A12 was labeled to QDs via the C-terminal cysteine for oriented (O) or via amino groups for random (R) conjugation. Although the orientation of the V$_H$H on the QD surface did not have any significant influence on the average distance (Supporting Figure S10), it should have an influence on biomarker recognition due to better accessibility of the V$_H$H binding site on the opposite end of the C-terminal cysteine. To verify this hypothesis and to compare the performance of the IgG, Fab, and V$_H$H systems for HER2 detection, we measured immunoassay calibration curves (Figure 4) and determined LODs (Table 3). Similar to the
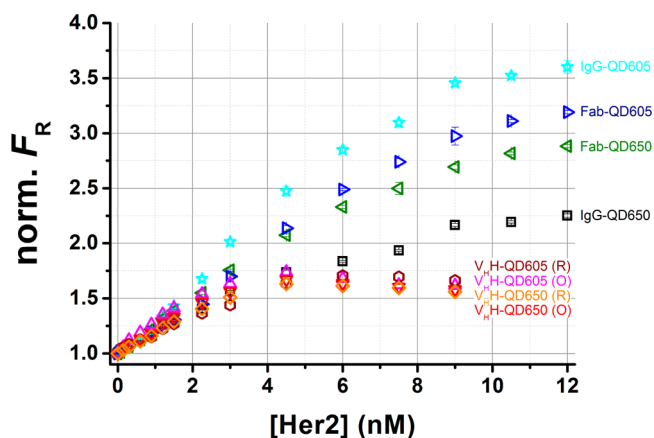
Figure 4. Homogeneous FRET immunoassay calibration curves against HER2 using different Tb−AB and AB−QD conjugates (blue, Tb-Tras/PertFab-QD605; green, Tb-Tras/PertFab-QD650; cyan, Tb-Tras/Pert-QD605; black, Tb-Tras/Pert-QD650; brown, Tb-Cys11A4/18A12-QD605; magenta, Tb-Cys11A4/18A12Cys-QD605; orange, Tb-Cys11A4/18A12-QD650; red, Tb-Cys11A4/18A12Cys-QD650). Individual curves for the Tb and QD signals (that lead to the calculation of F_R) and for the determination of LODs can be found in the Supporting Information (Supporting Figures S19−S26).

EGFR assays, all calibration curves showed a significant linear increase of F_R with increasing HER2 concentrations. The slopes (sensitivities) of all curves were quite similar in the linear part; however, the V$_H$H-based assays saturated at a lower concentration than the IgG and Fab-based assays, which led to a slightly reduced linear dynamic range. The inflection points of the V$_H$H curves were situated between ca. 3 and 4 nM HER2, which is slightly below the expected value of 4.5 nM (concentration of the recombinant human HER2 Fc chimera

**Table 3. Limits of Detection (LODs) of the Different HER2 Immunoassays**

AB combination	AB conjugate combination	LOD (nM)	LOD (ng/mL)	LOD (fmol)
IgG/IgG	Tb-Tras/Pert-QD650	0.09	19	4.6
	Tb-Tras/Pert-QD605	0.15	30	7.5
IgG/Fab	Tb-Tras/PertFab-QD650	0.11	23	5.6
	Tb-Tras/PertFab-QD605	0.12	23	5.8
V_HH/V_HH	Tb-Cys11A4/18A12Cys-QD605 (O)	0.04	8.0	2.0
	Tb-Cys11A4/18A12-QD605 (R)	0.12	24	6.1
	Tb-Cys11A4/18A12Cys-QD650 (O)	0.05	9.1	2.3
	Tb-Cys11A4/18A12-QD650 (R)	0.08	16	3.9

dimer) that corresponds to the beginning of Tb−AB saturation, as discussed for EGFR. This somewhat earlier saturation was most probably caused by an overestimation of the 11A4 V_HH concentrations (determined by UV−vis absorption spectroscopy) in the immunoassays. On the other hand, the IgG and Fab immunoassays saturated around 9 nM, which led to a larger linear dynamic range but a saturation concentration that was approximately 2-fold higher than expected from the Tb−AB concentrations. In contrast to Cet and Mat for EGFR, Tras and Pert bind to different domains of the HER2 monomer. The recombinant HER2 dimer used in our study may have led to

less accessible domains compared to the monomer, and therefore only one Tb−QD AB pair could bind per HER2 dimer. This 2-fold reduced AB recognition could explain the later saturation of the immunoassay calibration curves and led to a lower sensitivity and higher LODs compared to the IgG- and Fab-based assays for EGFR.

The LODs (Table 3) confirmed the lower FRET immunoassay performance of the Tras/Pert AB pair, most probably caused by the stronger nonspecific binding and the less efficient HER2 dimer recognition. Although all assays led to very low LODs in the 40 to 150 pM (8 to 30 ng/mL) HER2 range, the V_HH-based systems provided the lowest LODs. Oriented conjugation of V_HH on the QDs further improved the immunoassay performance. The LODs could be decreased significantly (ca. 2-fold for QD650 and 3-fold for QD605) and reached values of 8.0 and 9.1 ng/mL, which were below the suggested clinical cutoff level of 15 ng/mL HER2.[27,30] The concentration of soluble HER2 for breast cancer diagnostics was found to be in the 7−120 ng/mL range, but more than 3000 ng/mL were found for some metastatic patients.[27] Therefore, the automatic dilution function of the KRYPTOR plate reader would offer again a very useful advantage to increase the dynamic range for HER2 detection.

Duplexed EGFR/HER2 Immunoassay. Encouraged by the excellent results of the single-tumor marker assays, we aimed at demonstrating duplexed EGFR/HER2 detection from a single sample. Regarding the LODs (Tables 2 and 3), an optimal AB conjugate selection would be Tb-Cet/MatFab-QD650 for
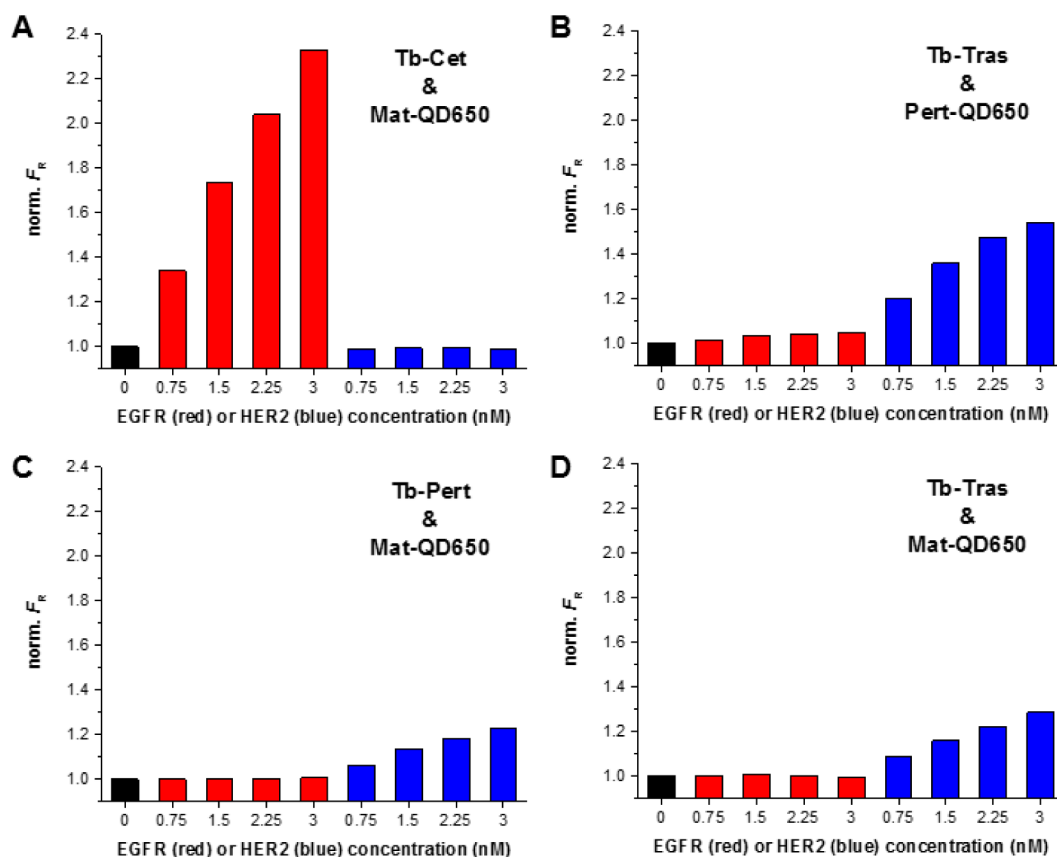
Figure 5. Specificity of the different AB pairs for EGFR (red) or HER2 (blue). Tb-Cet/Mat-QD650 (A) and Tb-Tras/Pert-QD650 (B) showed a concentration-dependent FRET-ratio increase only for their respective receptors. Tb-Pert/Mat-QD650 (C) and Tb-Tras/Mat-QD650 (D) showed a concentration-dependent FRET-ratio increase for HER2, which indicates a cross-reactivity of the EGFR-specific Mat to HER2. Tb-Cet/Pert-QD650 did not lead to any concentration dependent FRET-ratio increase (Supporting Figure S27).
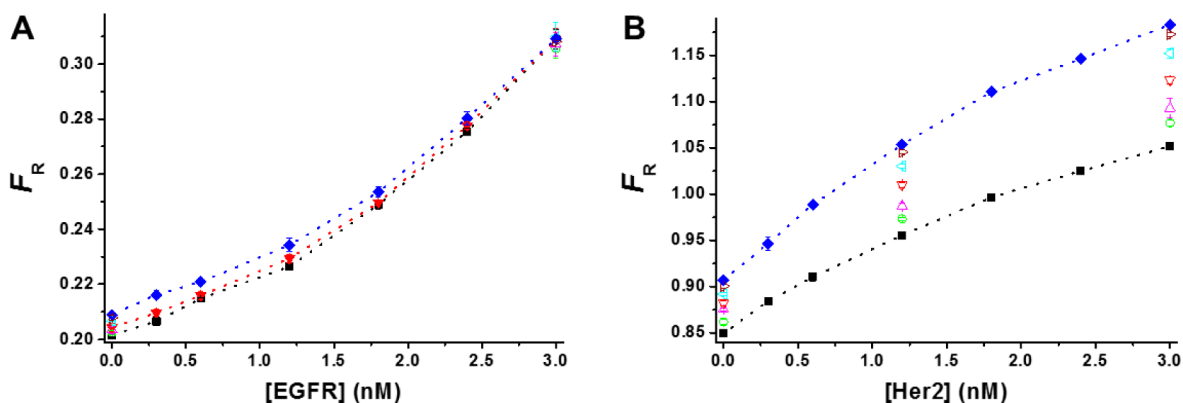
Figure 6. Duplexed immunoassay (all samples containing Tb-Cet, Tb-Tras, Mat-QD605, and Pert-QD650) calibration curves of EGFR (FRET-ratio of QD605 and Tb PL intensities, A) and HER2 (FRET-ratio of QD650 and Tb PL intensities, B) for increasing (0 nM, black; 0.3 nM, green; 0.6 nM, magenta; 1.2 nM, red; 1.8 nM, cyan; 2.4 nM, brown; 3 nM, blue) HER2 (A) and EGFR (B) concentrations.

EGFR and Tb-Cys11A4/18A12Cys-QD605 for HER2. However, this combination of Tb−IgG and Tb−V_HH in a duplexed assay imposes a significant drawback to the nanobody system. Because both assays used the same Tb as FRET donor and the Tb conjugation ratio on an IgG was much higher (8-fold) than on a V_HH, the Tb background signal in the V_HH-based assay would also strongly increase, which, in turn, would not lead to the same assay performance as for the optimized HER2 assay. Therefore, the best compromise for a duplexed assay was Tb-Cet/Mat-QD605 for EGFR and Tb-Tras/Pert-QD650 for HER2. Two important aspects need to be taken into consideration when developing multiplexed FRET biosensors: (*i*) optical crosstalk (due to overlapping QD emission spectra) and (*ii*) biological crosstalk (due to AB cross-reactivity to other biomarkers). While the first aspect was minimized by carefully selected bandpass filters for QD605 and QD650 PL detection (Figure 1B), the second one required evaluation of the AB specificity. To do so, we performed orthogonal experiments, in which all different EGFR (Cet and Mat) and HER2 (Tras and Pert) AB combinations were used in FRET immunoassays at different EGFR and HER2 concentrations. The dedicated AB pairs for EGFR (Cet and Mat, Figure 5A) and HER2 (Tras and Pert, Figure 5B) provided very specific FRET signals that were proportional to the concentration of their respective tumor markers and independent of the concentration of the nonspecific receptor. These results also showed the higher sensitivity (stronger concentration-dependent increase) of EGFR (Figure 5A) compared to HER2 (Figure 5B). Combining Cet and Pert did not lead to any antigen-specific signal, neither for EGFR nor for HER2 (Supporting Figure S27), which demonstrated their high specificity (very low cross-reactivity) for EGFR and HER2, respectively. On the other hand, combinations of Pert and Mat (Figure 5C) and Tras and Mat (Figure 5D) both resulted in slightly increasing FRET signals with increasing HER2 concentration, which revealed Mat cross-reactivity to HER2. Although the affinity of Mat to EGFR was much stronger (no influence of HER2 when Mat was used in combination with Cet, Figure 5A), the cross-reactivity of Mat to HER2 needed to be taken into account for the duplexed EGFR/HER2 immunoassay.

To evaluate the influence of cross-reactivity, we measured duplexed (Tb-Cet, Tb-Tras, Mat-QD605, and Pert-QD650 conjugates were all present in the samples) immunoassay calibration curves of EGFR at different HER2 concentrations (Figure 6A) and of HER2 at different EGFR concentrations

(Figure 6B). Due to the strong affinity of Cet and Mat to EGFR (Figure 5A) and the negligible cross-reactivity of Tras or Pert to EGFR (Supporting Figure S27), a variation of HER2 concentration in the assays did not significantly influence a precise EGFR detection (Figure 6A). Only for combinations of low EGFR and high HER2 concentrations did the cross-reactivity of Mat lead to an increased FRET-ratio signal, caused by FRET from Tb-Tras to Mat-QD605. The impact on HER2 detection was significantly stronger (Figure 6B). In this case, the cross-reactivity of Mat led to a competition with Tras and/or Pert for HER2, and the availability of free Mat-QD605 conjugates in the sample resulted in a decreased Tb-Tras-to-Pert-QD650 FRET ratio. The addition of EGFR led to a preferred binding of Mat to this growth factor receptor and reduced free Mat-QD605 that would have otherwise competed for HER2 binding. Consequently, an increasing EGFR concentration also resulted in more Tb-Tras-HER2-Pert-QD650 recognition and an increasing Tb-to-QD650 FRET ratio.

Because EGFR quantification was almost negligibly influenced by the presence of HER2 (Figure 6A), it could be used to correct the HER2 calibration curves from Figure 6B, which linearly increased with EGFR concentration. To verify this assumption, we prepared 19 samples with different EGFR and HER2 concentrations between 0 and 3 nM and performed duplexed immunoassays. First, EGFR concentrations were determined using the EGFR calibration curve without HER2 (black curve in Figure 6A). These EGFR concentrations were then used to adapt the HER2 calibration curve (EGFR concentration dependent curves from Figure 6B) to determine the HER2 concentrations. An additional correction factor (which can be calculated from the same calibration curves and is proportional to the HER2/EGFR concentration ratio) that took into account the deviations for combinations of high HER2 and low EGFR concentrations led to the final EGFR and HER2 concentrations in the duplexed assay. Because HER2 calibration curves need to be acquired for different EGFR concentrations (cf. Figure 6B), the calibration procedure for a duplexed EGFR/HER2 assay is slightly more laborious than for a single-marker assay. However, the duplexed assay itself is faster and less expensive because only one sample and one microplate-well are necessary for quantifying the concentrations of both ErbB receptors. As shown in Figure 7, the various combinations of different EGFR and HER2 concentrations could be determined very precisely, which demonstrated that a
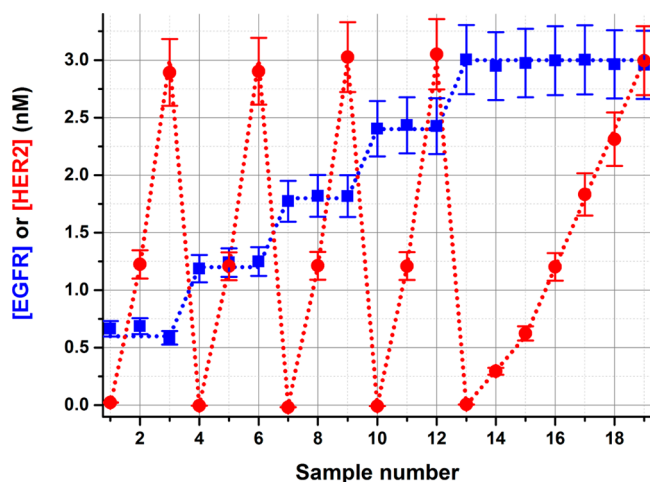
Figure 7. Duplexed FRET immunoassay for the quantification of EGFR (blue squares) and HER2 (red dots) within 19 different samples. Dotted lines represent the known concentrations, and data points represent the measured concentrations (±10% error bars).

specific and sensitive detection of both ErbB receptors within a single sample at low nanomolar concentrations is possible with FRET from one type of Tb complex to different QDs. This first demonstration of a homogeneous multiplexed FRET immunoassay with QD acceptors presents an important milestone for implementing such assays into widely applicable clinical diagnostics.

CONCLUSIONS

Many immunoassays that used QDs and FRET have been developed over the past two decades. Although profound investigations are essential to implementing novel nano-, photonic-, and biomaterial combinations into functional and commercial applications, a systematic study of various types of ABs and QDs for immunoassays of important biomarkers at clinically relevant concentrations and in multiplexing format has never been performed. Here, we have scrutinized the influence of AB sizes (IgGs, Fab fragments, and $V_H H$ fragments) and orientations (random and C-terminal conjugation of $V_H H$ to QDs), AB−QD conjugation ratios, and AB nonspecific binding and cross-reactivity on the performance of single and duplexed EGFR and HER2 immunoassays. The commercial therapeutic antibodies matuzumab, cetuximab, trastuzumab, and pertuzumab as well as four different $V_H H$ nanobodies (EgA1, EgB4, 11A4, and 18A12) were used in various combinations to demonstrate and compare homogeneous Tb-to-QD FRET immunoassays. Using the clinical fluorescence plate reader KRYPTOR, the single tumor marker assays showed the best results, using Tb-conjugated Cet IgG ABs and MatFab-conjugated QD650 with LODs of 2.9 ng/mL EGFR in a 50 μL sample volume. HER2 could be detected with the lowest LOD of 8.0 ng/mL, using Tb and QD605 conjugated in an oriented manner to the C-termini of 11A4 and 18A12 nanobodies. These results showed that QD-conjugation via cysteines, in the hinge region of IgGs or introduced to the C-termini of nanobodies, are the most promising AB-conjugation approaches. Although the LODs were much higher than for commercial heterogeneous ELISA, both detection limits were below the proposed clinical cutoff values of 45 and 15 ng/mL for EGFR and HER2, respectively. Therefore, the important advantages of simplicity and speed of the homogeneous FRET

assays compared to heterogeneous ELISA could lead to immediate benefits for clinical diagnostics. Moreover, the demonstration of duplexed EGFR/HER2 detection provided another unique selling point compared to the single-marker ELISA tests. Compared to other homogeneous multiplexed FRET immunoassays using dye acceptors,[45] QDs provide superior brightness and photostability and the unique advantage of not requiring any complicated correction procedures for spectral crosstalk, which also simplified correction of biological cross-reactivity in the present study. In conclusion, our systematic investigation of various antibody-quantum dot conjugation strategies for single and duplexed homogeneous clinical immunoassays against EGFR and HER2 presents an important benchmark for the implementation of QD−AB conjugates as functional and generic nanomaterials into clinical diagnostics.

■ MATERIALS AND METHODS

Materials. Recombinant human EGFR Fc chimera (#344-ER-050) and HER2 Fc chimera (#1129-ER-050) dimers were purchased from R&D system. Nanobodies against EGFR (EgA1 and EgB4) were produced as described elsewhere.[46] Nanobodies against HER2 (11A4-Cysteine-tag and 18A12-Cysteine-tag) were produced as described elsewhere.[35] IgGs against EGFR (cetuximab and matuzumab) were provided by Merck KGaA, Darmstadt (Germany). IgGs against HER2 (trastuzumab and pertuzumab) were provided by Genentech/Roche Diagnostics GmbH, Penzberg (Germany). Fab fragments were prepared using a Pierce Mouse IgG_1 Fab and F(ab')$_2$ preparation kit (Thermo Fisher Scientific). Fragments were verified using SDS-PAGE. Quantum dots (eFluor650/605 Nanocrystal Conjugation Kit—Sulfhydryl Reactive) were provided by Affymetrix/eBioscience. Terbium complexes (Lumi4-Tb-NHS and Lumi4-maleimide) were provided by Lumiphore. Sodium tetraborate decahydrate ($Na_2B_4O_7$·$10H_2O$), Trizma hydrochloride, phosphate buffered saline (1×PBS), sodium bicarbonate ($NaHCO_3$), hydrochloric acid (HCl), sodium hydroxide (NaOH), hydroxylamine hydrochloride ($HONH_2$·HCl), Tris(2-carboxyethyl) phospine hydrochloride (TCEP), dimethyl sulfoxide (DMSO), N,N-dimethylformamide (DMF), and bovine serum albumin (BSA) were purchased from Sigma-Aldrich. Sodium chloride (NaCl), disodium hydrogen phosphate dihydrate (Na_2HPO_4·$2H_2O$), and sodium dihydrogen phosphate dihydrate (NaH_2PO_4·$2H_2O$) were purchased from Duchefa. All chemicals were used as received. Newborn calf serum was provided by Cezanne/Thermo Fisher Scientific. Water was purified by Purelab Option-Q equipped with biofilter (ELGA Labwater Veolia water ST1, Antony, France) to produce nuclease free water.

QD Bioconjugates. Prior to conjugation, protected sulfhydryl groups (N-succinimidyl S-acetylthioacetate) were introduced to anti-EGFR nanobody EgB4 (no sulfhydryl groups available) at 5× molar excess using a SATA kit (#26102, Thermo Fisher Scientific). The sulfhydryl groups were deprotected by diacylation according to the manufacturer's protocol. For anti-EGFR antibodies cetuximab and matuzumab, anti-HER2 antibodies trastuzumab and pertuzumab, and anti-HER2 nanobodies 11A4 and 18A12 (for oriented labeling based on a terminal cysteine tags), no additional steps were necessary before conjugation. Sulfhydryl-activated antibody or nanobody solutions (in concentration excess to the QD solutions) were prepared in 1× PBS and conjugated to eFluor QDs according to the manufacturer's instructions. Unbound proteins were separated by washing three to four times in 100 kDa molecular weight cutoff (MWCO) spin columns (Millipore) with 100 mM sodium tetraborate buffer (pH 8.3) as a washing buffer. QD concentrations were determined by absorbance measurements using molar absorptivities of 1.1×10^6 M^{-1} cm^{-1} (at 641 nm) for QD650 and of 2.5×10^5 M^{-1} cm^{-1} (at 594 nm) for QD605 as provided by the manufacturer. Antibodies were quantified by absorbance measurements at 280 nm using an extinction coefficient of 1.4 g^{-1} L cm^{-1}, 2.4 g^{-1} L cm^{-1}, 2.2 g^{-1} L cm^{-1}, and 2.0 g^{-1} L cm^{-1} for antibodies (Cet, Mat, MatFab, Tras, Pert, PertFab), EgA1 (or

EgB4), 11A4, and 18A12, respectively. The labeling ratios were determined by linear combination of the respective absorbance values of QDs and antibodies within the QD antibody conjugates.

Tb Complex Bioconjugates. Lumi4-Tb-NHS was dissolved to 8 mM in anhydrous DMF and mixed (in concentration excess to the antibody solutions) with the antibody samples in 100 mM carbonate buffer at pH 9.0. The mixtures were incubated while rotating at 25 rpm (Intelli-Mixer, ELMI) for 2 h at room temperature. For Tb-conjugate purification, the samples were washed four to six times with 100 mM TRIS-Cl at pH 7.2 using 50 kDa MWCO spin columns for IgG, 10 kDa MWCO spin columns (Millipore) for Fab, and 3 kDa MWCO spin columns for V_HH conjugates. Anti-HER2 nanobody 11A4-cysteine was conjugated with Lumi4-maleimide, which was dissolved to 8 mM in anhydrous DMF. 11A4-Cysteine was first reduced by excess TCEP for 30 min at room temperature in reducing buffer (50 mM sodium phosphate, 150 mM NaCl, pH = 6.5), and then excess TCEP was washed three times with labeling buffer (50 mM sodium phosphate, 150 mM NaCl, pH = 7.4) using 3 kDa MWCO spin columns (Millipore). Reduced 11A4-Cysteine was mixed with excess Lumi4-maleimide for 3 h at room temperature in labeling buffer. For Lumi4–11A4 purification, the samples were washed four to six times with 100 mM TRIS-Cl at pH 7.4 using 3 kDa MWCO spin columns. Lumi4–11A4 was then charged with Tb^{3+} ions using a concentration excess of $TbCl_3$ for 1 h and being stored at 4 °C. Tb concentrations were determined by absorbance measurements at 340 nm using a molar absorptivity of 26 000 M^{-1} cm^{-1} as provided by the manufacturer. Antibodies were quantified by absorbance measurements at 280 nm. The conjugation ratios were determined by a linear combination of the respective absorbance values of Tb and antibodies within the Tb-antibody conjugates.

Photophysical Properties. Absorption spectra (Lambda 35 UV/vis System, PerkinElmer) and emission spectra (FluoTime 300, PicoQuant) were recorded in Tris(hydroxymethyl)-aminomethane (TRIS-Cl, Sigma-Aldrich) buffer with a pH of 7.4 and sodium-tetraborate buffer with a pH of 8.5 (Sigma-Aldrich) for Tb and QD samples, respectively. Förster distances were determined as described elsewhere.[21] PL decay curves were acquired directly from the FRET immunoassay samples on an EI fluorescence plate reader (Edinburgh Instruments) using 4000 detection bins of 2 μs integration time and nitrogen laser (VSL 337 ND, Spectra Physics) excitation (337.1 nm, 20 Hz). For intensity normalization of decay curves, each curve within one graph was multiplied by the value that resulted in unity intensity at 0.5 ms for the decay curve of the sum of only AB−QD and only Tb−AB. Optical transmission filter bandpass wavelengths were 494 ± 12 nm (Semrock) for the Tb detection channel, 659 ± 10 nm (Semrock) for the QD650 detection channel, and 608 ± 4 nm (Delta) for the QD605 detection channel.

Homogeneous FRET Immunoassays. The Tb and QD antibody conjugates were each dissolved in 50 μL of TRIS-Cl buffer containing 0.5% bovine serum albumin (BSA, Sigma-Aldrich). A total of 50 μL of EGFR or HER2 antigen samples with varying concentrations were added to the 100 μL solutions containing both the Tb and QD conjugates. Time-gated (0.1−0.9 ms) PL intensity measurements were acquired on a KRYPTOR compact plus fluorescence plate reader (Cezanne/Thermo Fisher Scientific) using 500 detection bins of 2 μs integration time and nitrogen laser excitation (337.1 nm, 20 Hz, 100 pulses). Optical transmission filter bandpass wavelengths were 494 ± 12 nm (Semrock) for the Tb detection channel, 659 ± 10 nm (Semrock) for the QD650 detection channel, and 608 ± 4 nm (Delta) for the QD605 detection channel. All FRET assays were measured in black 96-well microtiter plates with an optimal working volume of 150 μL. Each sample containing EGFR or HER2 antigen samples was prepared three times, and the samples without EGFR or HER2 were prepared 10 times. All samples were measured in triplicate. Error bars that are not visible in the graphs were smaller than the data points. After sample preparation, the microtiter plates were incubated for 180 min at 37 °C before measurements on the KRYPTOR and EI fluorescence plate readers.

ASSOCIATED CONTENT

Ⓢ Supporting Information

The Supporting Information is available free of charge on the ACS Publications website at DOI: 10.1021/acs.chemmater.6b03198.

> Overview of Tb and QD AB conjugation methods (Table S1), PL decay curves (Tb-donors and QD-acceptors) of all immunoassays (Figures S1−S10), EGFR immunoassay calibration curves for the Tb and QD signals and for the determination of LODs (Figures S11−S18), HER2 immunoassay curves for the Tb and QD signals and for the determination of LODs (Figures S19−S26), and specificity determination of Tb-Cet/Pert-QD650 (Figure S27) (PDF)

AUTHOR INFORMATION

Corresponding Author

*E-mail: niko.hildebrandt@u-psud.fr.

Present Address

∥CEA, INAC-SyMMES, 17 rue des Martyrs, F-38054 Grenoble Cedex 9, France

Notes

The authors declare no competing financial interest.

REFERENCES

(1) La Thangue, N. B.; Kerr, D. J. Predictive Biomarkers: A Paradigm Shift Towards Personalized Cancer Medicine. *Nat. Rev. Clin. Oncol.* **2011**, 8 (10), 587−596.

(2) Ong, F. S.; Das, K.; Wang, J.; Vakil, H.; Kuo, J. Z.; Blackwell, W.-L. B.; Lim, S. W.; Goodarzi, M. O.; Bernstein, K. E.; Rotter, J. I.; Grody, W. W. Personalized Medicine and Pharmacogenetic Biomarkers: Progress in Molecular Oncology Testing. *Expert Rev. Mol. Diagn.* **2012**, 12 (6), 593−602.

(3) Rusling, J. F.; Kumar, C. V.; Gutkind, J. S.; Patel, V. Measurement of Biomarker Proteins for Point-Of-Care Early Detection and Monitoring of Cancer. *Analyst* **2010**, 135 (10), 2496−2511.

(4) Ky, B.; French, B.; Levy, W. C.; Sweitzer, N. K.; Fang, J. C.; Wu, A. H. B.; Goldberg, L. R.; Jessup, M.; Cappola, T. P. Multiple Biomarkers for Risk Prediction in Chronic Heart Failure. *Circ.: Heart Failure* **2012**, 5 (2), 183−190.

(5) Richter, B.; Koller, L.; Hohensinner, P. J.; Zorn, G.; Brekalo, M.; Berger, R.; Moertl, D.; Maurer, G.; Pacher, R.; Huber, K.; Wojta, J.; Huelsmann, M.; Niessner, A. A Multi-Biomarker Risk Score Improves Prediction of Long-Term Mortality in Patients with Advanced Heart Failure. *Int. J. Cardiol.* **2013**, 168 (2), 1251−1257.

(6) Zethelius, B.; Berglund, L.; Sundstrom, J.; Ingelsson, E.; Basu, S.; Larsson, A.; Venge, P.; Arnlov, J. Use of Multiple Biomarkers to Improve the Prediction of Death from Cardiovascular Causes. *N. Engl. J. Med.* **2008**, 358 (20), 2107−2116.

(7) Wild, D. *The Immunoassay Handbook*, 4th ed.; Elsevier: Amsterdam, 2013.

(8) Hemmilä, I. LANCE: Homogeneous Assay Platform for HTS. *J. Biomol. Screening* **1999**, *4* (6), 303–307.

(9) Hemmilä, I.; Mukkala, V. M. Time-Resolution in Fluorometry Technologies, Labels, and Applications in Bioanalytical Assays. *Crit. Rev. Clin. Lab. Sci.* **2001**, *38* (6), 441–519.

(10) Mathis, G. HTRF Technology. *J. Biomol. Screening* **1999**, *4* (6), 309–313.

(11) Hildebrandt, N.; Wegner, K. D.; Algar, W. R. Luminescent Terbium Complexes: Superior Förster Resonance Energy Transfer Donors for Flexible and Sensitive Multiplexed Biosensing. *Coord. Chem. Rev.* **2014**, *273*, 125–138.

(12) Avvakumova, S.; Colombo, M.; Tortora, P.; Prosperi, D. Biotechnological Approaches toward Nanoparticle Biofunctionalization. *Trends Biotechnol.* **2014**, *32* (1), 11–20.

(13) Geißler, D.; Hildebrandt, N. Recent Developments in FRET Diagnostics Using Quantum Dots. *Anal. Bioanal. Chem.* **2016**, *408*, 4475–4483.

(14) Han, S. W.; Jang, E.; Koh, W. G. Microfluidic-Based Multiplex Immunoassay System Integrated with an Array of QD-Encoded Microbeads. *Sens. Actuators, B* **2015**, *209*, 242–251.

(15) Liu, D.; Wu, F.; Zhou, C. H.; Shen, H. B.; Yuan, H.; Du, Z. L.; Ma, L.; Li, L. S. Multiplexed Immunoassay Biosensor for the Detection of Serum Biomarkers - Beta-HCG and AFP of Down Syndrome Based on Photoluminescent Water-Soluble Cdse/Zns Quantum Dots. *Sens. Actuators, B* **2013**, *186*, 235–243.

(16) Zhou, J. W.; Lei, L. M.; Liang, Q. N.; Liu, T. C.; Lin, G. F.; Dong, Z. N.; Liang, R. L.; Chen, Z. H.; Wu, Y. S. Dual-labeled time-resolved immunofluorometric assay for the determination of IgM antibodies to rubella virus and cytomegalovirus in human serum. *Clin. Biochem.* **2015**, *48* (9), 603–608.

(17) Chen, M. J.; Wu, Y. S.; Lin, G. F.; Hou, J. Y.; Li, M.; Liu, T. C. Quantum-Dot-Based Homogeneous Time-Resolved Fluoroimmunoassay of Alpha-Fetoprotein. *Anal. Chim. Acta* **2012**, *741*, 100–105.

(18) Geißler, D.; Linden, S.; Liermann, K.; Wegner, K. D.; Charbonnière, L. J.; Hildebrandt, N. Lanthanides and Quantum Dots as Förster Resonance Energy Transfer Agents for Diagnostics and Cellular Imaging. *Inorg. Chem.* **2014**, *53* (4), 1824–1838.

(19) Chen, Z. H.; Wu, Y. S.; Chen, M. J.; Hou, J. Y.; Ren, Z. Q.; Sun, D.; Liu, T. C. A Novel Homogeneous Time-Resolved Fluoroimmunoassay for Carcinoembryonic Antigen Based on Water-Soluble Quantum Dots. *J. Fluoresc.* **2013**, *23* (4), 649–657.

(20) Bhuckory, S.; Lefebvre, O.; Qiu, X.; Wegner, K. D.; Hildebrandt, N. Evaluating Quantum Dot Performance in Homogeneous FRET Immunoassays for Prostate Specific Antigen. *Sensors* **2016**, *16* (2), 197.

(21) Wegner, K. D.; Jin, Z. W.; Linden, S.; Jennings, T. L.; Hildebrandt, N. Quantum-Dot-Based Förster Resonance Energy Transfer Immunoassay for Sensitive Clinical Diagnostics of Low-Volume Serum Samples. *ACS Nano* **2013**, *7* (8), 7411–7419.

(22) Wegner, K. D.; Linden, S.; Jin, Z. W.; Jennings, T. L.; el Khoulati, R.; van Bergen en Henegouwen, P. M. P.; Hildebrandt, N. Nanobodies and Nanocrystals: Highly Sensitive Quantum Dot-Based Homogeneous FRET Immunoassay for Serum-Based EGFR Detection. *Small* **2014**, *10* (4), 734–740.

(23) Geißler, D.; Charbonnière, L. J.; Ziessel, R. F.; Butlin, N. G.; Löhmannsröben, H.-G.; Hildebrandt, N. Quantum Dot Biosensors for Ultrasensitive Multiplexed Diagnostics. *Angew. Chem., Int. Ed.* **2010**, *49* (8), 1396–1401.

(24) Gazdar, A. F. Epidermal Growth Factor Receptor Inhibition in Lung Cancer: The Evolving Role of Individualized Therapy. *Cancer Metastasis Rev.* **2010**, *29* (1), 37–48.

(25) Weigel, M. T.; Dowsett, M. Current and Emerging Biomarkers in Breast Cancer: Prognosis and Prediction. *Endocr.-Relat. Cancer* **2010**, *17* (4), R245–R262.

(26) Yamashita-Kashima, Y.; Iijima, S.; Yorozu, K.; Furugaki, K.; Kurasawa, M.; Ohta, M.; Fujimoto-Ouchi, K. Pertuzumab in Combination with Trastuzumab Shows Significantly Enhanced Antitumor Activity in HER2-Positive Human Gastric Cancer Xenograft Models. *Clin. Cancer Res.* **2011**, *17* (15), 5060–5070.

(27) Asgeirsson, K. S.; Agrawal, A.; Allen, C.; Hitch, A.; Ellis, I. O.; Chapman, C.; Cheung, K. L.; Robertson, J. F. R. Serum Epidermal Growth Factor Receptor and HER2 Expression in Primary and Metastatic Breast Cancer Patients. *Breast Cancer Res.* **2007**, *9* (6), R75.

(28) Hirsch, F. R.; Varella-Garcia, M.; Cappuzzo, F. Predictive Value of EGFR and HER2 Overexpression in Advanced Non-Small-Cell Lung Cancer. *Oncogene* **2009**, *28*, S32–S37.

(29) Milanezi, F.; Carvalho, S.; Schmitt, F. C. EGFR/HER2 in Breast Cancer: A Biological Approach for Molecular Diagnosis and Therapy. *Expert Rev. Mol. Diagn.* **2008**, *8* (4), 417–434.

(30) Müller, V.; Witzel, I.; Pantel, K.; Krenkel, S.; Lück, H. J.; Neumann, R.; Keller, T.; Dittmer, I.; Jänicke, F.; Thomssen, C. Prognostic and Predictive Impact of Soluble Epidermal Growth Factor Receptor (Segfr) Protein in the Serum of Patients Treated with Chemotherapy for Metastatic Breast Cancer. *Anticancer Res.* **2006**, *26* (2B), 1479–1487.

(31) Lee, C. M.; Shrieve, D. C.; Zempolich, K. A.; Lee, R. J.; Hammond, E.; Handrahan, D. L.; Gaffney, D. K. Correlation between Human Epidermal Growth Factor Receptor Family (EGFR, HER2, HER3, HER4), Phosphorylated Akt (P-Akt), and Clinical Outcomes after Radiation Therapy in Carcinoma of the Cervix. *Gynecol. Oncol.* **2005**, *99* (2), 415–421.

(32) Sapsford, K. E.; Algar, W. R.; Berti, L.; Gemmill, K. B.; Casey, B. J.; Oh, E.; Stewart, M. H.; Medintz, I. L. Functionalizing Nanoparticles with Biological Molecules: Developing Chemistries that Facilitate Nanotechnology. *Chem. Rev.* **2013**, *113* (3), 1904–2074.

(33) Brazhnik, K.; Nabiev, I.; Sukhanova, A. Oriented Conjugation of Single-Domain Antibodies and Quantum Dots. *Methods Mol. Biol. (N. Y., NY, U. S.)* **2014**, *1199*, 129–140.

(34) Hofman, E. G.; Ruonala, M. O.; Bader, A. N.; van den Heuvel, D.; Voortman, J.; Roovers, R. C.; Verkleij, A. J.; Gerritsen, H. C.; van Bergen en Henegouwen, P. M. P. EGF Induces Coalescence of Different Lipid Rafts. *J. Cell Sci.* **2008**, *121* (15), 2519–2528.

(35) Kijanka, M.; Warnders, F.-J.; El Khattabi, M.; Lub-de Hooge, M.; van Dam, G. M.; Ntziachristos, V.; de Vries, L.; Oliveira, S.; van Bergen en Henegouwen, P. M. P. Rapid Optical Imaging of Human Breast Tumour Xenografts Using Anti-HER2 VHHs Site-Directly Conjugated to Irdye 800CW for Image-Guided Surgery. *Eur. J. Nucl. Med. Mol. Imaging* **2013**, *40* (11), 1718–1729.

(36) Jennings, T. L.; Becker-Catania, S. G.; Triulzi, R. C.; Tao, G.; Scott, B.; Sapsford, K. E.; Spindel, S.; Oh, E.; Jain, V.; Delehanty, J. B.; Prasuhn, D. E.; Boeneman, K.; Algar, W. R.; Medintz, I. L. Reactive Semiconductor Nanocrystals for Chemoselective Biolabeling and Multiplexed Analysis. *ACS Nano* **2011**, *5* (7), 5579–5593.

(37) Marx, J. L. Antibody Structure: Now in Three Dimensions. *Science* **1975**, *189* (4208), 1075–1077.

(38) Revets, H.; De Baetselier, P.; Muyldermans, S. Nanobodies as Novel Agents for Cancer Therapy. *Expert Opin. Biol. Ther.* **2005**, *5* (1), 111–124.

(39) Guddat, L. W.; Herron, J. N.; Edmundson, A. B. 3-Dimensional Structure of a Human-Immunoglobulin with a Hinge Deletion. *Proc. Natl. Acad. Sci. U. S. A.* **1993**, *90* (9), 4271–4275.

(40) Wegner, K. D.; Morgner, F.; Oh, E.; Goswami, R.; Susumu, K.; Stewart, M. H.; Medintz, I. L.; Hildebrandt, N. Three-Dimensional Solution-Phase Förster Resonance Energy Transfer Analysis of Nanomolar Quantum Dot Bioconjugates with Subnanometer Resolution. *Chem. Mater.* **2014**, *26* (14), 4299–4312.

(41) Wegner, K. D.; Lanh, P. T.; Jennings, T.; Oh, E.; Jain, V.; Fairclough, S. M.; Smith, J. M.; Giovanelli, E.; Lequeux, N.; Pons, T.; Hildebrandt, N. Influence of Luminescence Quantum Yield, Surface Coating, and Functionalization of Quantum Dots on the Sensitivity of Time-Resolved FRET Bioassays. *ACS Appl. Mater. Interfaces* **2013**, *5*, 2881–2892.

(42) Zhang, X.; Zhang, L.; Tong, H. M.; Peng, B.; Rames, M. J.; Zhang, S. L.; Ren, G. 3D Structural Fluctuation of IgG1 Antibody Revealed by Individual Particle Electron Tomography. *Sci. Rep.* **2015**, *5*, 9803.

(43) Schmiedel, J.; Blaukat, A.; Li, S.; Knoechel, T.; Ferguson, K. M. Matuzumab Binding to EGFR Prevents the Conformational

Rearrangement Required for Dimerization. *Cancer Cell* **2008**, *13* (4), 365−373.

(44) Schmitz, K. R.; Bagchi, A.; Roovers, R. C.; van Bergen en Henegouwen, P. M. P.; Ferguson, K. M. Structural Evaluation of EGFR Inhibition Mechanisms for Nanobodies/VHH Domains. *Structure* **2013**, *21* (7), 1214−1224.

(45) Geißler, D.; Stufler, S.; Löhmannsröben, H.-G.; Hildebrandt, N. Six-Color Time-Resolved Förster Resonance Energy Transfer for Ultrasensitive Multiplexed Biosensing. *J. Am. Chem. Soc.* **2013**, *135* (3), 1102−1109.

(46) Roovers, R. C.; Laeremans, T.; Huang, L.; De Taeye, S.; Verkleij, A. J.; Revets, H.; de Haard, H. J.; van Bergen en Henegouwen, P. M. P. Efficient Inhibition of EGFR Signalling and of Tumour Growth by Antagonistic Anti-EGFR Nanobodies. *Cancer Immunol. Immunother.* **2007**, *56* (3), 303−317.